

# A Novel Titania-based Photocatalyst for Water Purification

Elena Savinkina, Galina Kuzmicheva, and Lyubov Obolenskaya

**Abstract**—The recently reported nanosize  $\eta$ -modification of titanium dioxide was studied as a photocatalyst for water purification. Its synthesis was modified to increase the yield up to 95% and prepare the particles with variable parameters. The photocatalytic activity of  $\eta$ -TiO<sub>2</sub>, which was studied in the model reactions of dye degradation under UV radiation, strongly depends on crystallite size, pre-treatment of the samples, and pH. It increases with the increase of pH and retains on multiply usage.

**Keywords**—Hydrolysis, Nanosize particles, Photocatalysis, Titanium dioxide, Metastable titania.

## I. INTRODUCTION

WATER and air pollution has been a problem throughout history. Efficient water use is an environmental priority in all countries of the world [1]. Water quality is directly influenced by the surrounding environment's features [2]. Air pollutants are responsible for the acidification of water ecosystems and eutrophication of waters [3]. The methods used for water purification include physical, biological and chemical processes. Among various water purification and recycling technologies, adsorption is a fast, inexpensive and universal method [4, 5]. In recent years, semiconductor photocatalytic process has shown a great potential as a low-cost, environmental friendly and sustainable treatment technology to align with the "zero" waste scheme in the water/wastewater industry [6]. During the last decade, titanium dioxide (titania, TiO<sub>2</sub>) nanoparticles have emerged as promising photocatalysts for water purification, water treatment, air cleaning, etc. [7, 8].

Titanium dioxide is known to form 12 modifications (including high pressure forms and metastable forms produced synthetically). The stable rutile and brookite and metastable anatase occur in nature as well-known minerals and can be prepared in both bulk and nanosize forms. Rutile, anatase and

brookite all contain six coordinated titanium (Fig. 1). Titania is the most widely used white pigment. In recent years, preparation, modification, and applications (Fig. 2) of TiO<sub>2</sub> nanosize modifications attract interest of many researchers [10, 11]. Titanium dioxide is the promising photocatalyst due to the most efficient photoactivity, highest stability, lowest cost, and absence of toxicity [12].

A considerable technique and academic interest in the photocatalytic properties of nanosize TiO<sub>2</sub> has led to many detailed studies of photodegradation of dyes and the related kinetics and mechanism study [13]–[19]. The release of colored waste waters containing dyes lost in the dyeing processes in textile industry is a considerable source of pollution. Traditional physic-chemical techniques just transfer organic compounds from water to another phase, causing a secondary pollution. The most suitable solution of the problem is the complete destruction of the contaminants with heterogeneous photocatalysis (using TiO<sub>2</sub> as a photocatalyst) which can be carried under ambient conditions (atmospheric oxygen) and may lead to complete mineralization of organic carbon into CO<sub>2</sub> [13].

In many works, commercial photocatalysts Hombikat UV 100 (pure anatase crystalline form) and Degussa P-25 (anatase and rutile mixture in 3–4 : 1 ratio) were studied. Numerous attempts to create more efficient photocatalysts resulted in maximally twofold accelerating the degradation of organic dyes as compared to Degussa P-25 showing the highest photocatalytic activity [13]–[19].

Several factors were found to accelerate the reactions catalyzed by TiO<sub>2</sub> [13]–[19]: the increase of the temperature of annealing the samples (higher degree of crystallinity); optimal sizes of particles varying in the 7–10 nm range (the best ratio of the rates for the bulk and surface recombination of the electron–hole pair); decrease of pH (protonation of the surface Ti–OH groups influencing the dye adsorption).

Recently, the new metastable  $\eta$ -modification of titanium dioxide was first synthesized (with yield <30%) as a nanosize powder with high adsorption properties [20]. Further study of  $\eta$ -TiO<sub>2</sub> [21]–[24] showed availability of good (photo)catalytic activity for this modification.

Therefore, the purpose of the work was to modify the synthesis of  $\eta$ -TiO<sub>2</sub> for increasing its yield and quality and to study its photocatalytic activity in relation to various factors.

Manuscript received

This work was supported by the Russian Foundation for Basic Research, project no. 10-03-00160.

E. V. Savinkina is with the Department of Inorganic Chemistry, Lomonosov University of Fine Chemical Technology, Moscow, Russian Federation (phone: 7-495-936-8912; fax: 7-495-434-8711; e-mail: e.savinkina@mail.ru).

G. M. Kuzmicheva is with the Department of Physics and Chemistry of Solids, Lomonosov University of Fine Chemical Technology, Moscow, Russian Federation (e-mail: galkuz@mitht.ru).

L. N. Obolenskaya is with the Lomonosov University of Fine Chemical Technology, Moscow, Russian Federation (e-mail: urraa@rambler.ru).

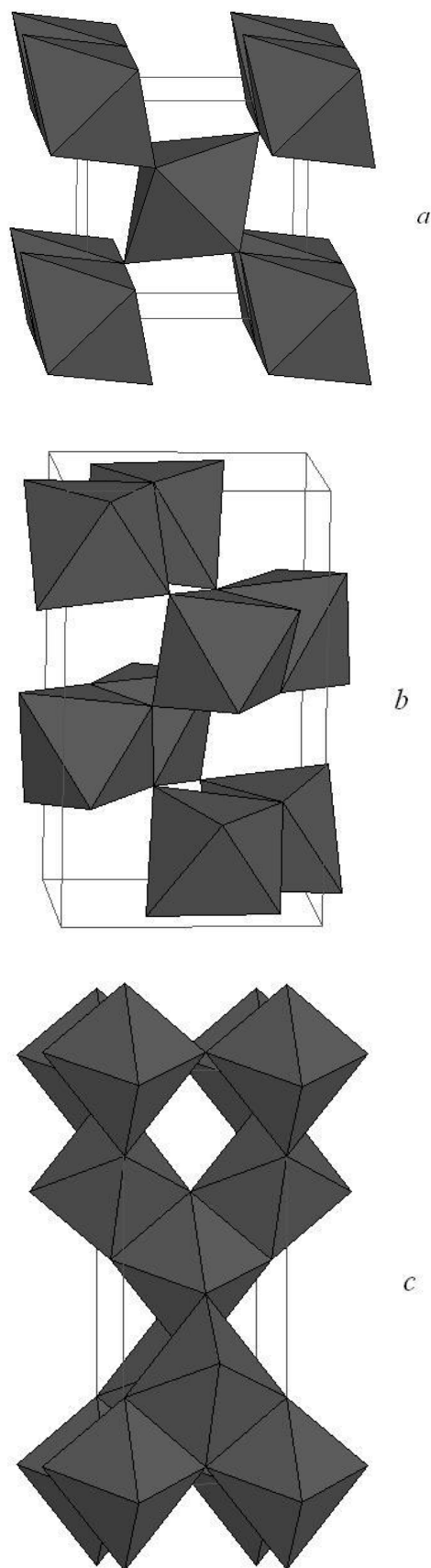


Fig. 1. The crystal structures of rutile (a), brookite (b), and anatase (c). [9]

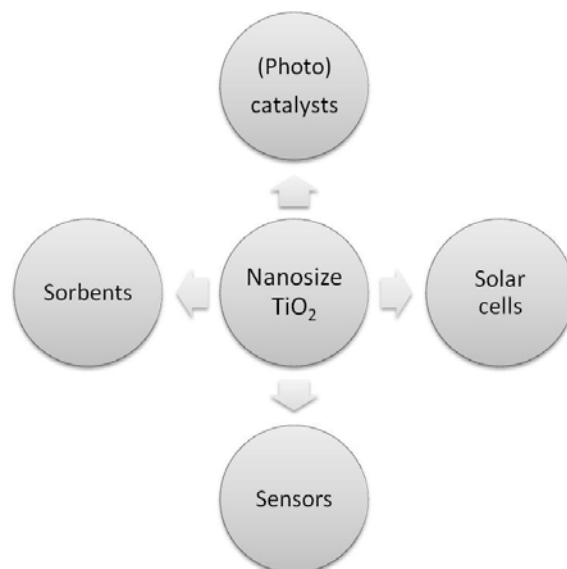


Fig. 2. Applications of nanosize TiO<sub>2</sub>.

## II. EXPERIMENTAL

### A. Synthesis

Commercial titanium oxysulfate–sulfuric acid complex hydrate (Aldrich) was used as an initial reagent without further purification. The reported technique of preparing  $\eta$ -TiO<sub>2</sub> by TiOSO<sub>4</sub> hydrolysis [20] could not assure high yield and appropriate morphology of the product; therefore we varied initial concentration of the reagent and synthesis conditions: temperature, heating rate and duration, stirring rate, nature and quantity of a coagulant, and final treatment of the solid (for more details, see Results and Discussion). In a typical experiment, the initial reagent was stirred in water (mass ratio TiOSO<sub>4</sub>·xH<sub>2</sub>SO<sub>4</sub>·yH<sub>2</sub>O : H<sub>2</sub>O = 1 : 6) under heating up to 90°C until complete dissolution; the reaction mixture was allowed to stay at this temperature for several minutes till light coagulation; then the KCl solution was added (8.5 mole per one mole Ti<sup>IV</sup>); the resulting solid was filtered off, washed with water and acetone and dried at 90°C for 1 h. Yield 95%.

### B. Characterization

All the samples were characterized by X-ray diffraction (XRD) patterns, which were collected on HZG-4 (Ni filter) and DRON-3 (diffracted-beam flat graphite monochromator) powder diffractometers (CuK<sub>α</sub> radiation, sample rotation, angular range 2θ = 2°–80°, step scan mode with a counting time of 10 s per data point and a scan step of 0.02°). The intensity data set was reduced using the PROFILE FITTING V 4.0 software package. Qualitative XRD phase analyses were carried out using JCPDS PDF-2, RETRIEVE, and earlier data.

Electron micrographs and electron diffraction patterns were obtained on a JEOL JEM 2100 high-resolution transmission electron microscope (TEM) (LaB6 cathode as an electron source; accelerating voltage, 200 kV; minimum electron beam diameter in transmission mode, 20 nm; specimen tilts of ±60° about the *x* axis and ±25° about the *y* axis; point and line

resolutions of 2.3 and 1.4 E, respectively; maximum accelerating voltage, 200 kV; direct magnification up to  $1.5 \times 106\times$ ).

Thermal analysis was carried out with a DTAS-1300 DSC instrument.

The particle (crystallite) size  $L$  was evaluated using the Scherrer formula:  $L = 0.9\lambda/\beta\cos\theta$ , where  $\lambda$  is the X-ray wavelength,  $2\theta \approx 25^\circ$ ,  $\beta = \sqrt{B^2 - b^2}$  is the physical width of the diffraction peak from the phase of interest (diffraction line profiles were fitted with Gaussians),  $B$  is the measured integral breadth of the peak, and  $b \approx 0.14^\circ$  is the instrumental correction obtained with an  $\alpha\text{-Al}_2\text{O}_3$  standard. The standard deviation was  $\pm 5\%$ .

The free specific surface area of the samples  $S$  was determined by the Brunauer–Emmett–Teller (BET) method from low-temperature nitrogen adsorption.

Aggregation kinetics was studied by the dynamic light-scattering method with the use of laser analyzer with high-sensitive photomultiplier (DelsaNano,  $\lambda = 658$  nm). The  $\zeta$  potential was measured with the same instrument.

IR spectra were recorded with an Infracum FT-02 spectrometer in nujol.

Electronic absorption spectra were recorded with an Aquilon CF 103 UV/vis spectrophotometer.

### C. Photocatalysis

Properties of the  $\eta\text{-TiO}_2$  samples was studied in the model reactions of photocatalytic degradation for color removal from aqueous solution containing organic dyes methyl orange (4-dimethylaminoazobenzene-4'-sulfonic acid sodium salt), xylenol orange (3,3'-bis[N,N-bis(carboxymethyl)-aminomethyl]-o-cresolsulfonephthalein tetrasodium salt), and methylene blue (3,7-bis(dimethylamino)phenothiazin-5-ium chloride) under illumination of UV light (UFO-V-4, DRT-125 mercury lamp,  $\lambda = 250\text{--}400$  nm,  $E = 3.11\text{--}4.97$  eV) in a photoreactor system with continuous stirring. The depth and surface of the solution were 0.04 m and 0.09 m<sup>2</sup>, respectively. In a typical experiment, the  $\eta\text{-TiO}_2$  powder was added into aqueous solution of a dye; the initial dye concentration and the amount of  $\eta\text{-TiO}_2$  concentrations were set at 0.33–1.04 M and 2.5–5.0 M, respectively; pH varied in the 1–9 range. The dye degradation was monitored by absorbance at  $\lambda = 490\text{--}510$  and 450–470 nm for methyl orange and xylenol orange in acidic and neutral solutions, respectively, and at  $\lambda = 550\text{--}590$  nm for methylene blue.

## III. RESULTS AND DISCUSSION

### A. Characterization of $\eta\text{-TiO}_2$

The X-ray diffraction data for the samples are indicative of nanoscale modification of titanium dioxide with  $\eta\text{-TiO}_2$  structure. The specific X-ray feature of  $\eta\text{-TiO}_2$  is a strong diffraction reflection at  $2\theta \sim 4.7^\circ\text{--}5.2^\circ$  with an interplanar distance of  $d \sim 20(5)$  Å and the presence of peaks at  $2\theta \sim 25^\circ$ ,  $33^\circ$ , and  $48^\circ$  [20] (Fig. 3).

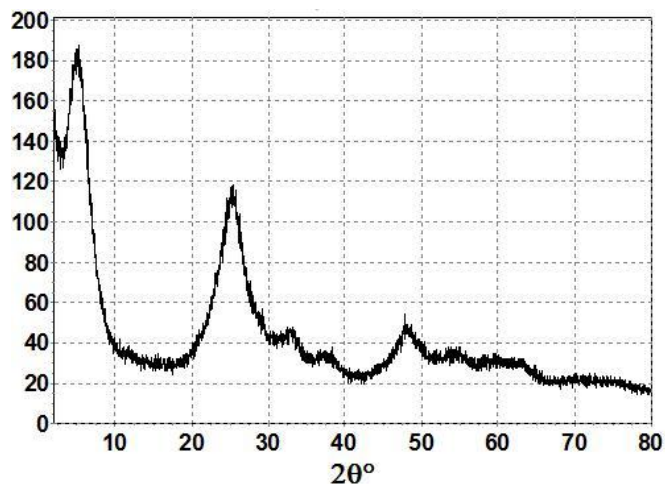


Fig. 3. X-Ray powder diffraction pattern of  $\eta\text{-TiO}_2$ .

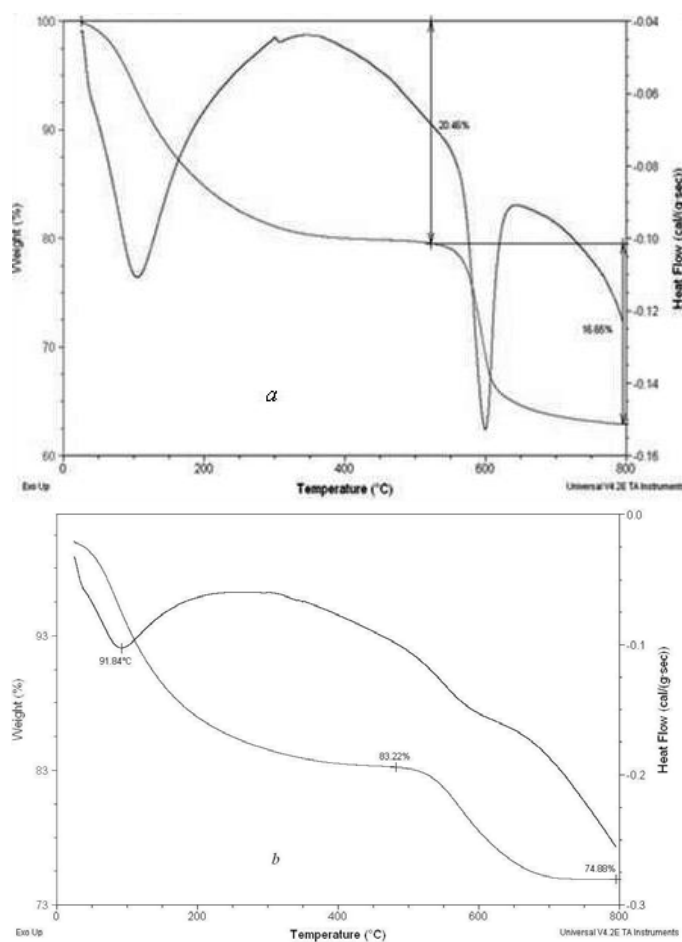


Fig. 4. Thermal curves for  $\eta\text{-TiO}_2$  (a) and anatase (b).

The  $\eta\text{-TiO}_2$  phase seems to be metastable, and its structure can be derivative from the anatase structure; small changes in conditions of the  $\eta\text{-TiO}_2$  preparation lead to the formation of a metastable phase with the anatase structure, and the  $\eta\text{-TiO}_2$  phase precedes the formation of this phase [23]. Thermal curves for  $\eta\text{-TiO}_2$  and anatase (Fig. 4) differ by an endothermal effect at  $\sim 650^\circ\text{C}$  which can be assigned to a phase transfer from the  $\eta\text{-TiO}_2$  to anatase modification.

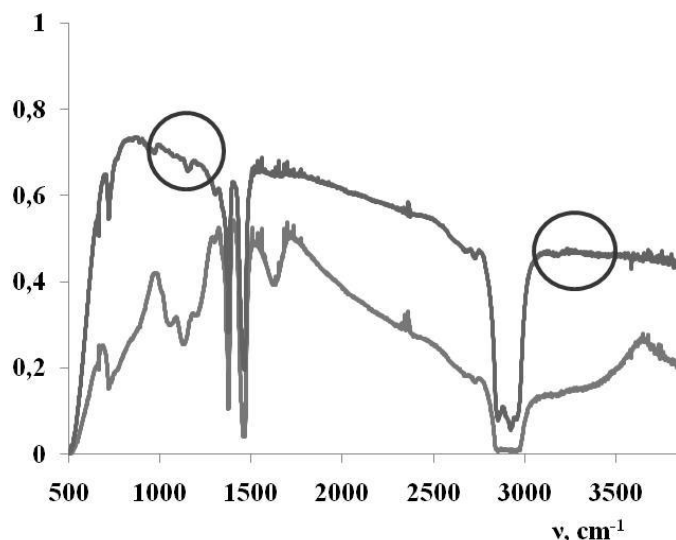


Fig. 5. IR spectra of  $\eta$ -TiO<sub>2</sub> before (1) and after (2) heating at 800°C. Circles show disappearance of the  $\delta$ (TiOH) and  $\nu$ (OH) modes at  $\sim 1100$  cm<sup>-1</sup> and  $\sim 3300$  cm<sup>-1</sup>, respectively.

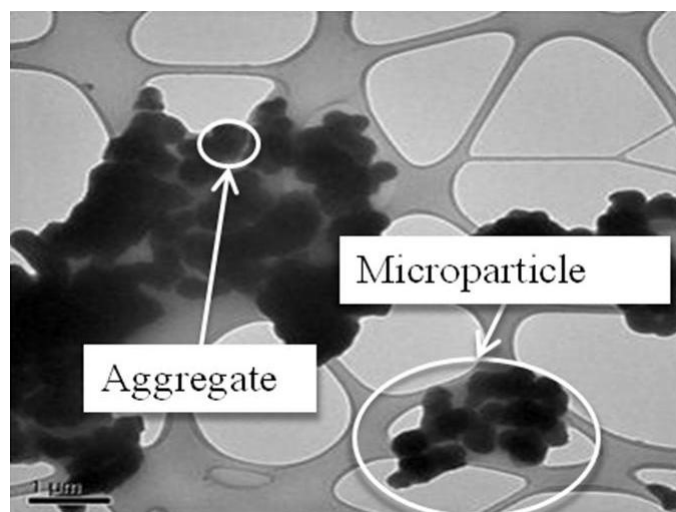


Fig. 6. TEM micrograph of the  $\eta$ -TiO<sub>2</sub> aggregates.

Two-stage mass loss is caused by removal of water molecules, which are weakly (the first stage) and strongly (the second stage) bonded to the titania surface. The water removal is supported by IR spectroscopy (Fig. 5). Bands assigned to vibrations of the surface hydroxyl groups disappear under heating.

However, a prolonged storage in air (for at least half a year) of samples with  $\eta$ -TiO<sub>2</sub> does not cause changes in the diffraction picture, which is evidence of its relative stability.

The crystallite size ( $L$ ) for  $\eta$ -TiO<sub>2</sub> is varied in the 3–6 nm range by changing reagent concentration, temperature, and synthesis duration. Nanoparticles of  $\eta$ -TiO<sub>2</sub> (8–14 nm in size [24]) tend to form agglomerates covered with an amorphous shell (Fig. 6). According to BET data, the free specific surface area is 4–18.0 m<sup>2</sup>/g, and ultrapour size is 0.002–0.004 cm<sup>3</sup>/g. The IR spectra show that the surface of the  $\eta$ -TiO<sub>2</sub> samples is hydrated and hydroxylated [23].

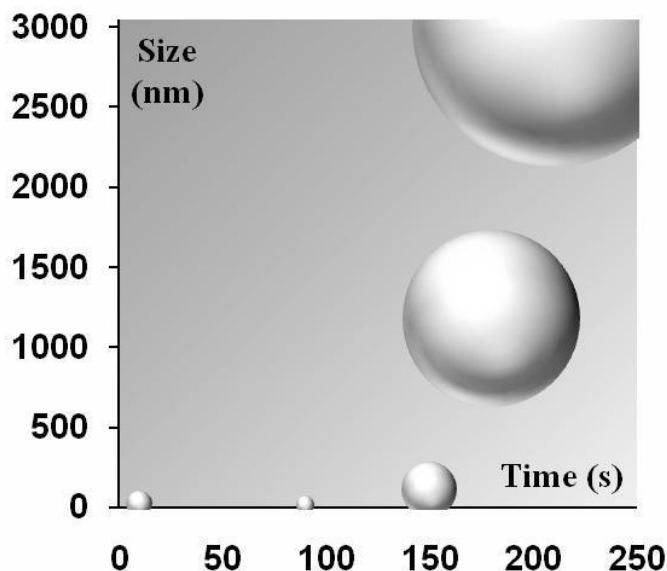


Fig. 7. Aggregation kinetics in the reaction mixture: 0.54 M Ti(IV), 298 K, index of refraction 1.3328, dynamic viscosity 0.8878 cp.

An important characteristic of titanium dioxide is the bandgap. For nanosize particles, it increases by  $\sim 0.05$ – $0.2$  eV relative to bulk rutile and anatase (3.03 and 3.18 eV, respectively); photocatalytic activity of both rutile and anatase increases with increase in BET surface area and with the magnitude of the blue shift in the bandgap [25]. The bandgap for the  $\eta$ -TiO<sub>2</sub> nanoparticles was calculated from the UV spectra of sols prepared by re-dispersion of synthesized powders as described in [27], [28]. Plots of  $(\alpha E)^{1/2}$  vs.  $E$ , where  $E$  is an energy of the UV absorption band and  $\alpha$  is calculated as  $\alpha = 2.303 \cdot I \cdot \rho \cdot (l \cdot c)^{-1}$ , where  $I$  is absorbance intensity,  $\rho$  is TiO<sub>2</sub> density,  $c$  is the loading of the colloid, and  $l$  is the path length) gave straight lines; their intercepts are ascribed to the bandgap absorption edge of titania. Its value (3.65–3.77 eV) is higher than for bulk anatase.

#### B. Synthesis Conditions

The titanyl sulfate hydrolysis in dilute solutions begins just after its contact with water (Fig. 7).

To record the UV spectrum of non-hydrolyzed TiOSO<sub>4</sub>, we used icy water (Fig. 8, curve 1). The spectrum changed immediately at room temperature indicating disappearance of titanyl and formation of a TiO<sub>2</sub> sol (Fig. 8, curves 2–9). Rapid spectral changes occurred during the first 30 min of the hydrolysis, after which minor absorption spectral changes were noted. Heating led to the noticeable decrease of the absorption (Fig. 8, curves 10–12), indicating further hydrolysis.

A shift of the UV absorption edge correlates with the particle size [28]. Therefore, we can conclude that the growth of the TiO<sub>2</sub> nanoparticles stops in first 30 min of the TiOSO<sub>4</sub> hydrolysis at room temperature resulting in formation of stable sols, which can be destroyed under heating or by adding coagulants. In [20], the coagulation of  $\eta$ -TiO<sub>2</sub> was caused by addition of HCl. However, the yield of the product prepared by the technique reported in [20] is not high.

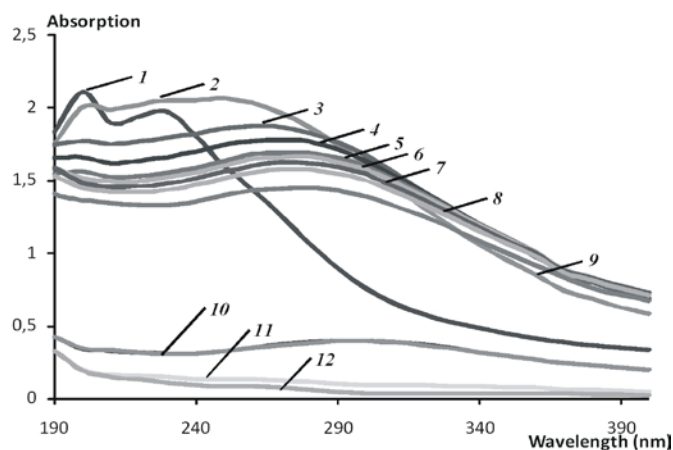


Fig. 8. UV spectra of TiOSO<sub>4</sub> ( $6.8 \cdot 10^{-4}$  M): unhydrolyzed (1); hydrolyzed at 20–25°C for 0 (2), 10 (3), 20 (4), 34 (5), 40 (6), 50 (7), 60 (8), 87 (9) min; hydrolyzed at 20–25°C for 80 min with one-fold (10), two-fold (11), and three-fold (12) heating up to 75°C.

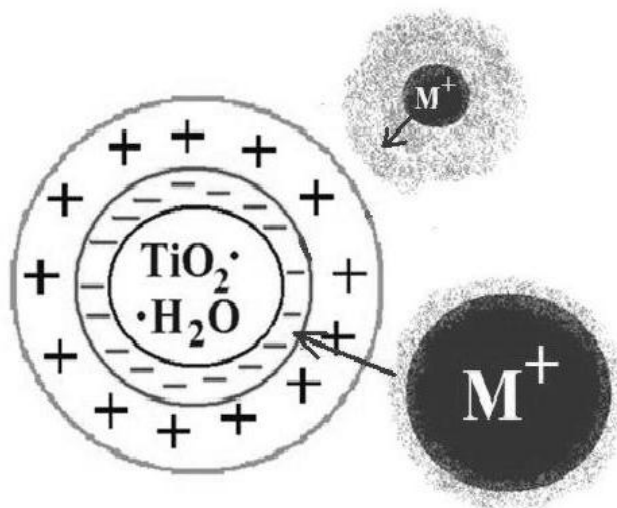


Fig. 9. Scheme of titania coagulation.

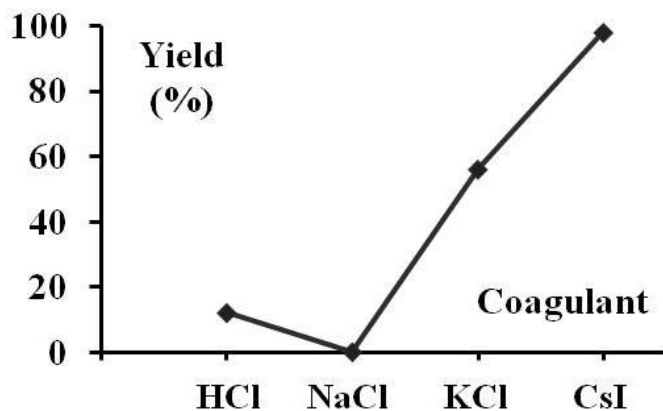


Fig. 10. Dependence of the yield on the coagulant nature.

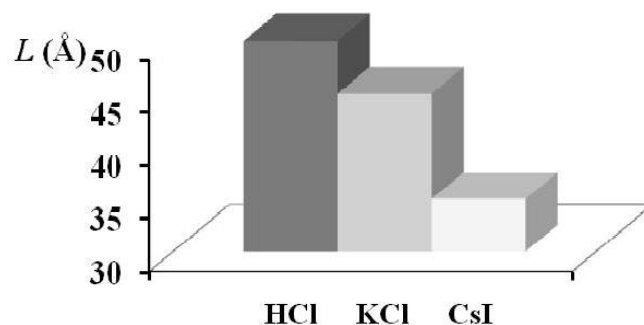


Fig. 11. Dependence of the crystallite size on the coagulant nature.

Increasing the  $\eta$ -TiO<sub>2</sub> yield is a difficult task since an enhancement of the TiOSO<sub>4</sub> hydrolysis leads to formation of the more stable anatase phase. Therefore, the main way for ruling the  $\eta$ -TiO<sub>2</sub> yield is affecting its coagulation (Fig. 9).

We tested a number of coagulants and found the best results for alkali-metal halides, namely KCl and CsI (Fig. 10).

Slight variations of other conditions (higher temperature or the coagulant : Ti<sup>IV</sup> ratio and lower TiOSO<sub>4</sub> concentration) can also increase the product yield; the yield is independent of hydrolysis duration, stirring, volume of a coagulant solution, and anion nature.

Since the yield is strongly dependent on the cation nature of the coagulant, the counterion layer in the coagulated particles must carry a negative charge. The  $\zeta$  potential (–50.2 mV) fits the  $\zeta$  potential range permitting coagulation (–30–70 mV).

Such factors as the heating rate, hydrolysis duration, maximal temperature and the coagulant nature have a strong effect on the crystallite size of the product. It is noteworthy that varying the coagulant in the HCl–KCl–CsI row simultaneously increases the yield of the product and decreases the crystallite size (Fig. 11). The additional coagulant quantity enlarges the yield but has no effect on the crystallite size. All other parameters increasing the yield lead to the increase of the crystallite size.

The samples with the optimal crystallite size of 4 nm (see below) can be prepared under the following conditions: initial concentration of TiOSO<sub>4</sub>, 0.67 M; heating rate, 8 deg/min; hydrolysis duration, 6–10 min; KCl : Ti(IV) ratio, 8.5 : 1.

### C. Photocatalytic Properties of $\eta$ -TiO<sub>2</sub>

The photocatalytic decolorization of the dyes (Fig. 12) can be described by the first order kinetic model,  $\ln(c_0/c) = kt$ , where  $c_0$  is the initial concentration and  $c$  is the concentration at time  $t$ ; the correlation constant for the fitted line was calculated to be  $R^2 = 0.91–0.99$  (Fig 13). This is supported by independence of the reaction rate of the  $\eta$ -TiO<sub>2</sub> content and its increase with the increase of the dye concentration. After mixing the initial components, the dye decolorization begins after an induction period (15–30 min). The induction period disappears on pre-stirring the  $\eta$ -TiO<sub>2</sub> suspension for 30 min followed by addition of a dye or by ultrasonic pre-treatment of the reaction mixture. Pre-dispersion of the sample with either ultrasound or stirring increases the reaction rate (Fig. 14).

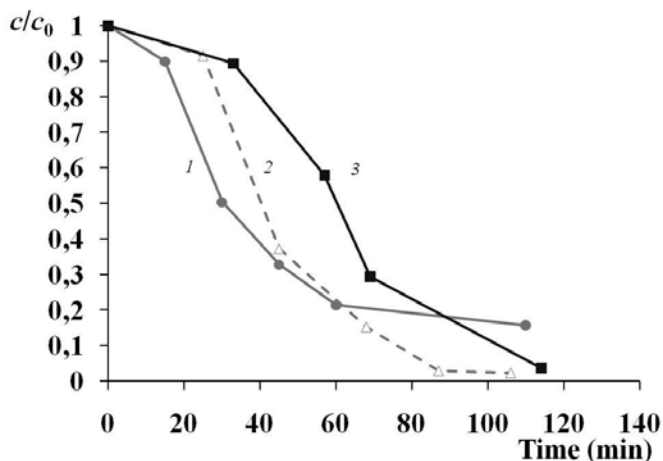


Fig. 12. Kinetic curves for decolorization of xlenol orange (1), methyl orange (2) and methylene blue (3).

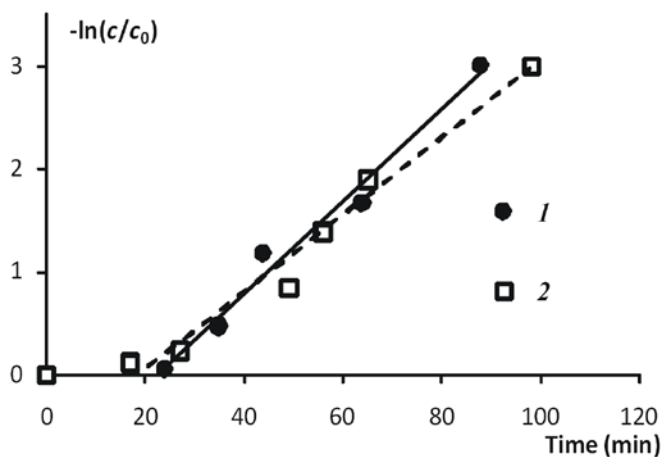


Fig. 13. Photocatalytic decomposition first order kinetics profiles of methyl orange,  $c_0 = 1.04$  M, pH 2 (1) and methylene blue,  $c_0 = 0.33$  M, pH 5 (2).

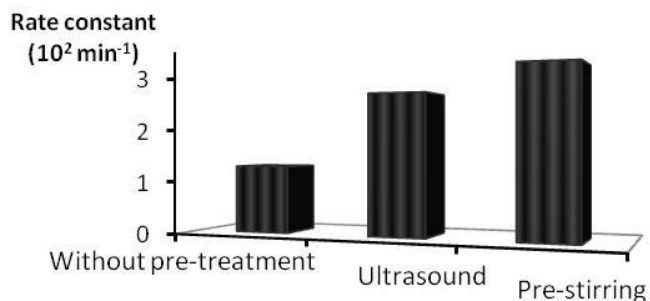


Fig. 14. Dependence of rate constant on pre-treatment of  $\eta$ -TiO<sub>2</sub> for photocatalytic decolorization of methylene blue.

In contrast to nanosize anatase and its mixtures with rutile [13]–[17], photocatalytic activity of the  $\eta$ -TiO<sub>2</sub> samples noticeably increases with the increase of pH (Fig. 15), especially for methylene blue. It is noteworthy that decomposition of methylene blue proceeds only in neutral and alkaline solutions.

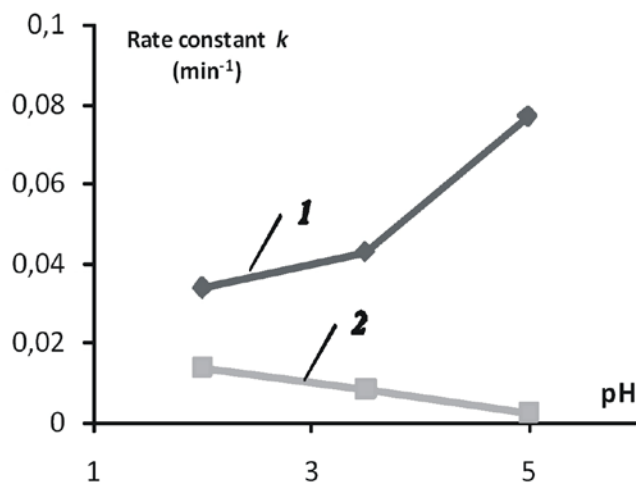


Fig. 15. First-order kinetics rate constant ( $k$ ) of methyl orange decomposition vs. pH for  $\eta$ -TiO<sub>2</sub> (1) and Degussa P25 [13] (2).

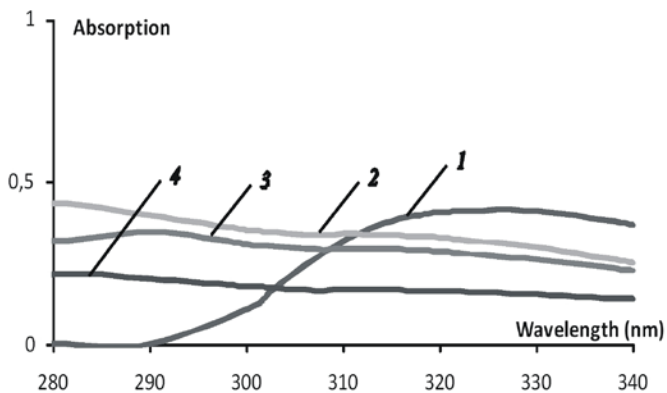


Fig. 16. UV spectra of  $\eta$ -TiO<sub>2</sub> sols sampled from the reaction mixture in 0 (1), 30 (2), 64 (3), and 94 min (4), pH 3.

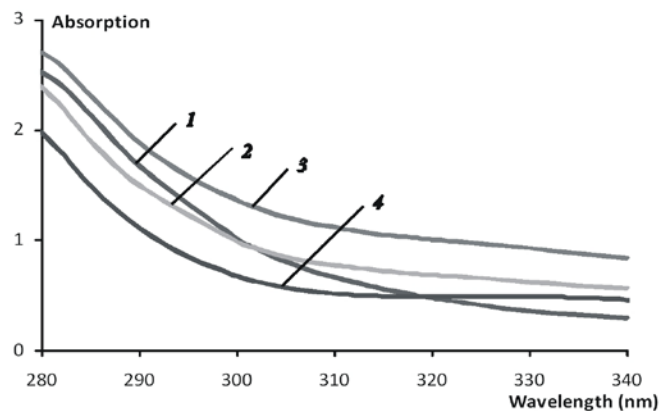


Fig. 17. UV spectra of  $\eta$ -TiO<sub>2</sub> sols sampled from the reaction mixture in 0 (1), 25 (2), 55 (3), and 85 min (4), pH 11.

Occurrence of the induction period and high photocatalytic activity at pH > 3 may be caused by destruction of agglomerates where crystallites are joined with an amorphous interlayer. It seems that pre-dispersion and/or alkalization of the reaction mixture facilitate dissolution of the amorphous interlayer resulting in formation of smaller  $\eta$ -TiO<sub>2</sub> particles.

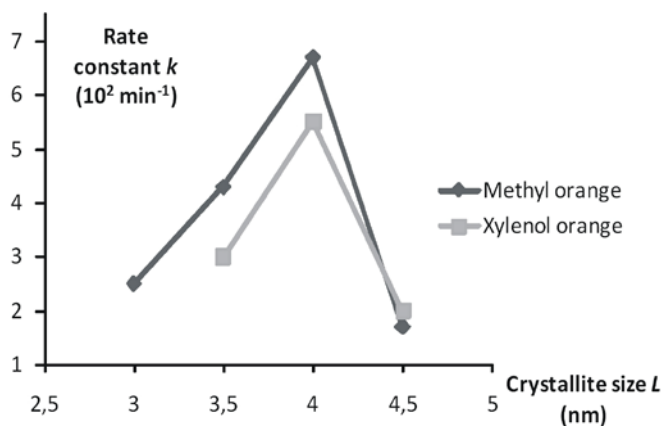


Fig. 18. First-order kinetics rate constant ( $k$ ) of dye decomposition vs. crystallite size ( $L$ ) for  $\eta$ -TiO<sub>2</sub>.

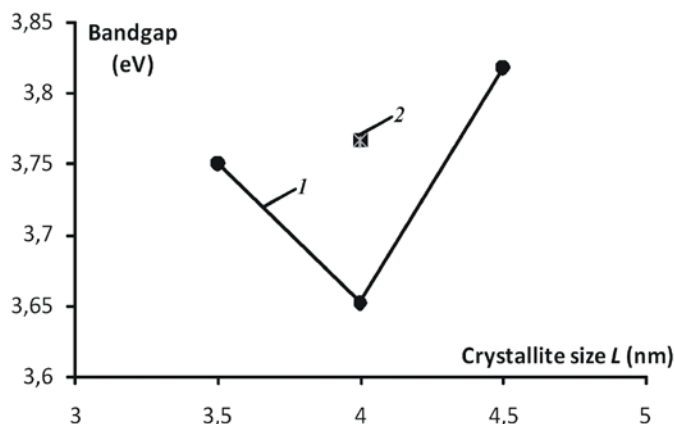


Fig. 19. Bandgap for re-dispersed particles vs. crystallite size ( $L$ ) for  $\eta$ -TiO<sub>2</sub>, coagulated with an alkali-metal halide (1) and HCl (2).

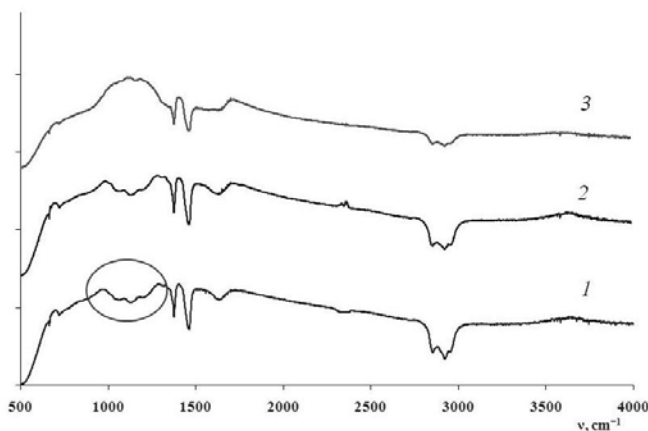


Fig. 20. IR spectra of  $\eta$ -TiO<sub>2</sub> before photoreaction (1) and after photoreaction at pH < 7 (2) and > 7 (3). The circle shows the band of  $\delta$ (TiOH) at  $\sim 1100$  cm<sup>-1</sup>

It leads to enlargement of the catalyst surface contacting with the dye solution. This fact is supported by UV spectra of the acidic and alkaline reaction solutions (Figs. 16, 17). Absorption by nanosize particles is noticeably higher at pH 11 than at pH 3.

The rate of the dye decolorization is maximal for the

samples where the  $\eta$ -TiO<sub>2</sub> crystallites are 4 nm in size (Fig. 18). The same crystallite size corresponds to the minimal bandgap (Fig. 19) for the  $\eta$ -TiO<sub>2</sub> particles.

Frequencies and intensities of the bands assigned to the active -OH groups on the  $\eta$ -TiO<sub>2</sub> surface ( $\sim 1100$  cm<sup>-1</sup>,  $\delta$ TiOH;  $\sim 3300$  cm<sup>-1</sup>,  $\nu$ OH) in the IR spectra of the samples do not change after their use in the reaction of the dye photodestruction (Fig. 20).

This indicates regeneration of the active groups on the surface and therefore possibility of multiple utilization of the photocatalyst. Direct measurements showed no decrease of the rate constant after the two-fold use of a sample.

#### IV. CONCLUSION

We were able to synthesize the recently reported nanosize  $\eta$ -modification of titanium dioxide with yields up to 95% and to examine its photocatalytic activity.

In addition to higher yield (as compared to the earlier reported synthesis of  $\eta$ -TiO<sub>2</sub> [20]), the number of stages is diminished (5 instead of 7), duration of energy-losing stages is shortened (80 min instead of 170 min), use of the HCl and NaOH concentrated solutions is excluded.

Depending on conditions, the sizes of  $\eta$ -TiO<sub>2</sub> crystallites, nanoparticles, spherical particles and agglomerates vary in the 3–6, 8–14, 200–300 and 900–1000 nm ranges, respectively. The photocatalytic activity of  $\eta$ -TiO<sub>2</sub> depends on crystallite sizes, pre-treatment of the samples, and pH. The unique properties of  $\eta$ -TiO<sub>2</sub> can be caused by its formation under mild synthetic conditions; the small uniform crystallites are combined in aggregates by amorphous layers protecting them from contact with environment and destroying under prolonged stirring, ultrasound and/or high pH.

The  $\eta$ -modification of titanium dioxide can be combined with SiO<sub>2</sub>, Pt, Cu, etc. for better (photo)catalytic properties.

#### REFERENCES

- [1] A. Silva-Afonso, F. Rodrigues, and C. Pimentel-Rodrigues, "Assessing the impact of water efficiency in energy efficiency and reducing GHG emissions: A case study," *Int. J. Energy Environ.*, vol. 5, no. 4, pp. 541–548, 2011.
- [2] L. Ghervase, C. Ioja, E. M. Carstea, L. Niculita, D. Savastru, G. Pavelescu, and G. Vanau, "Evaluation of lentic ecosystems from Bucharest City," *Int. J. Energy Environ.*, vol. 5, no. 2, pp. 183–192, 2011.
- [3] C. Arapatsakos, "The three way catalyst efficiency increase," *Int. J. Energy Environ.*, vol. 3, no. 2, pp. 69–76, 2009.
- [4] Imran Ali and V. K. Gupta, "Advances in water treatment by adsorption technology," *Nature Protocols*, vol. 1, no. 6, pp. 2661–2667, 2007.
- [5] P. Sampranpi boon, and P. Charkeikong, "Equilibrium isotherm, thermodynamic and kinetic studies of lead adsorption onto pineapple and paper waste sludges," *Int. J. Energy Environ.*, vol. 4, no. 3, pp. 88–98, 2010.
- [6] M. N. Chong, B. Jin, C. W. Chow, C. Saint, "Recent developments in photocatalytic water treatment technology: a review," *Water Res.*, vol. 44, no. 10, pp. 2997–3027, May 2010.
- [7] A.A. Adesina, "Industrial exploitation of photocatalysis progress, perspectives and prospects," *Catal. Surv. Asia*, vol. 8, no. 4, pp. 265–273, 2004.

- [8] N. Savage and M. S. Diallo, "Nanomaterials and water purification: Opportunities and challenges," *J. Nanoparticle Res.*, vol. 7, nos. 4–5, pp. 331–342, May 2005.
- [9] <http://ruby.colorado.edu/~smyth/min/tio2.html>
- [10] S. M. Lam, J. C. Sin and A. R. Mohamed, "Recent patents on photocatalysis over nanosized titanium dioxide," *Recent Patents on Chemical Engineering*, vol. 1, no. 3, pp. 209–219, July 2008.
- [11] X. Chen and S. S. Mao, "Titanium dioxide nanomaterials: synthesis, properties, modifications, and applications," *Chem. Rev.*, vol. 107, pp. 2891–2959, June 2007
- [12] K. Hashimoto, H. Irie, and A. Fujishima, "TiO<sub>2</sub> photocatalysis: a historical overview and future prospects," *AAPPS Bulletin*, vol. 17, pp. 12–29, December 2007.
- [13] N. Guettaï and H. Ait Amar, "Photocatalytic oxidation of methyl orange in presence of titanium dioxide in aqueous suspension. Part I: Parametric study," *Desalination*, vol. 185, pp. 427–437, April 2005.
- [14] N. Guettaï and H. Ait Amar, "Photocatalytic oxidation of methyl orange in presence of titanium dioxide in aqueous suspension. Part II: Kinetics study," *Desalination*, vol. 185, pp. 439–448, April 2005.
- [15] M. N. Rashed and A. A. El-Amin, "Photocatalytic degradation of methyl orange in aqueous TiO<sub>2</sub> under different solar irradiation sources," *Int. J. Phys. Sci.*, vol. 2, pp. 073–081, March 2007.
- [16] N. Barka, S. Qourzal, A. Assabbane, and Y. Ait-Ichou, "Kinetic modeling of the photocatalytic degradation of methyl orange by supported TiO<sub>2</sub>," *J. Environmental Sci. Eng.*, vol. 4, pp.1–5, May 2010.
- [17] Yao J., Wang Ch., "Decolorization of methylene blue with TiO<sub>2</sub> sol via UV irradiation photocatalytic degradation," *Int. J. Photoenergy*, vol. 2010, ID 643182, 6 pp., June 2010.
- [18] A. R. Khataea and M. B. Kasiri, "Photocatalytic degradation of organic dyes in the presence of nanostructured titanium dioxide: Influence of the chemical structure of dyes," *J. Mol. Catalysis A: Chemical*, vol. 328, pp. 8–26, June 2010.
- [19] A. Hosseinnia, M. Keyanpour-Rad, and M. Pazouki, "Photo-catalytic degradation of organic dyes with different chromophores by synthesized nanosize TiO<sub>2</sub> particles," *World Applied Sci. J.*, vol. 8, pp. 1327–1332, November 2010.
- [20] M. Dadachov, "Novel titanium dioxide, process of making and method of using same," U.S. Patent 0171877, August 3, 2006.
- [21] G. M. Kuz'micheva, E. V. Savinkina, L. N. Obolenskaya, L. I. Belogorokhova, B. N. Mavrin, M. G. Chernobrovkin and A. I. Belogorokhov, "Synthesis, characterization, and properties of nanoscale titanium dioxide modifications with anatase and η-TiO<sub>2</sub> structures," *Crystallography Reports*, vol. 55, pp. 866–871, May 2010.
- [22] E. V. Savinkina, G. M. Kuz'micheva, N. Yu. Tabachkova, L. N. Obolenskaya, P. A. Demina, and A. G. Yakovenko, "Synthesis and morphology of anatase and η-TiO<sub>2</sub> nanoparticles," *Inorg. Mater.*, vol. 47, pp. 489–494, May 2011.
- [23] G. M. Kuz'micheva, E. V. Savinkina, L. I. Belogorokhova, B. N. Mavrin, V. R. Flid, A. G. Yakovenko, and A. I. Belogorokhov, "The characteristics of the nanosized η-TiO<sub>2</sub> polymorph," *Rus. J. Phys. Chem. A*, vol. 85, pp. 1037–1040, June 2011.
- [24] G. M. Kuz'micheva, E. V. Savinkina, M. G. Chernobrovkin, D. N. Titov, P. A. Demina, L. N. Obolenskaya, L. G. Bruk, and A. G. Yakovenko, "Composition, microstructure, and properties of anatase and η-TiO<sub>2</sub> nanoparticles," *Inorg. Mater.*, vol. 47, pp. 753–758, July 2011.
- [25] M. Anpo, T. Shima, S. Kodama, and Y. Kubokawa, "Photocatalytic hydrogenation of propyne with water on small-particle titania: size quantization effects and reaction intermediates," *J. Phys. Chem.*, vol. 91, pp 4305–4310, July 1987.
- [26] N. Serpone, D. Lawless, and R. Khairutdinov, "Size effects on the photophysical properties of colloidal anatase TiO<sub>2</sub> particles: size quantization versus direct transitions in this indirect semiconductor?" *J. Phys. Chem.*, vol. 99, pp. 16646–16654, November 1995.
- [27] A. M. Peiró, J. Peral, C. Domingo, X. Domènech, and J. A. Ayllón, "Low-temperature deposition of TiO<sub>2</sub> thin films with photocatalytic activity from colloidal anatase aqueous solutions," *Chem. Mat.*, vol. 13, pp. 2567–2573, July 2001.
- [28] C. Kormann, D. W. Bahnemann, and M. R. Hoffmann, "Preparation and characterization of quantum-size titanium dioxide," *J. Phys. Chem.*, vol. 92, pp. 5196–5201, September 1988.